

Matador PedalSports: N.E.D. 1.0

Final Design Report

ASME Human Powered Vehicle Challenge



2010

Abstract

Human powered vehicles (HPVs) come in many different sizes and configurations. A human powered vehicle can be as simple as a paddle boat and as complex as an airplane. HPVs include vehicles built for air, water, or ground transport, but the common denominator is the integration of a human into the design. They optimize the human's strengths and compensate for their weaknesses. The primary purpose of a human powered ground vehicle is to transport its rider and cargo safely and efficiently. A human powered ground vehicle in its most simple sense is the traditional bicycle. However, the requirements of the HPV Challenge tend to encourage other vehicle configurations. This design report will detail the design of a three-wheeled recumbent vehicle which is intended to excel in all aspects of the HPVC. Anything that transports, supports, and includes humans needs to be analyzed and tested thoroughly before being put into production. Thus finite element analysis (FEA) as well as physical testing was performed to ensure the safety of the rider as well as possible pedestrians around the vehicle.

Table of Contents

Page

Introduction.....	4
Biomechanics.....	4-5
Design Description.....	5-13
Materials Science and Testing.....	13-18
Design Analysis	18-24
Fluid Flow Analysis	24-26
Cost Analysis	26-27

Introduction

The 2009-2010 California State University, Northridge (CSUN) Human Powered Vehicle Team is the fifth consecutive team to participate in the ASME Human Powered Vehicle Challenge. Last year was a landmark year for the Matador PedalSports team. The team achieved a fourth place finish in the competition with a clean sheet design, which is our highest placing to date. The 2009 vehicle was a partially faired composite upright bicycle. This road style vehicle performed exceptionally well in the speed endurance event with a first place finish. While the vehicle performed very well during the endurance event its sprint capabilities were lacking. The exposed rider and minimal fairing provided a high drag coefficient which was detrimental to the vehicle's top speed.

This year's human powered vehicle is also a clean sheet design. The team has analyzed our past vehicles; looking at advantages, disadvantages, as well as innovations made. This year the team has designed a structural belly-pan that is made from carbon fiber composite materials as well as a structural aramid honeycomb core. The vehicle configuration is a partially faired recumbent tricycle, with two wheels in the front that will provide steering and one single wheel in the rear that will provide forward motion (also known as a tadpole recumbent). The vehicle has been designed to be lightweight as well as very stable and can be seen in Figure 1a and 1b. Multiple software packages as well as physical testing were used to design and analyze this year's vehicle. The SolidWorks CAD and simulation package was the primary design and analysis tool used. It was used to create a

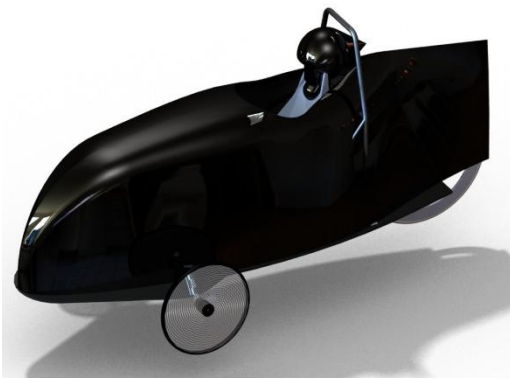


Figure 1a: Vehicle Rendering with Fairing



Figure 1b: Vehicle Rendering without Fairing

solid model of the entire vehicle assembly, and perform Finite Element Analysis (FEA) and Computational Fluid Dynamics (CFD) analysis. In addition to the SolidWorks simulation package NEI Nastran was used to analyze the structural belly-pan, which was complemented with physical testing. The measurement standard when designing the vehicle was the SI system. The cycling industry uses the SI measurement system; therefore by using the SI system of measurements the team ensured proper fit and alignment of all purchased components. The only exception to this rule is measurements and calculations made from physical testing. Since the U.S. uses the English system of measurement all testing components and fixtures are calibrated for English units; for this reason physical testing results and calculations were performed using the English system. The full design process can also be found at

www.ecs.csun.edu/hpv/csun2010home.

Bio-Mechanics

Bio-mechanics combines engineering mechanics with biological systems. It focuses on the physical human interactions with the machine. While a rider's fitness and training is enormously important, designing the vehicle around the rider is just as important. Before any portion of the vehicle could be designed this

year’s riders needed to be identified from among the team members. Preliminary rider tryouts were held using a similar tadpole recumbent HPV from a previous year. A PowerTap device was installed on the rear wheel to measure a rider’s power output in Watts, similar to dynamometers that measure a car’s horsepower. Through the PowerTap measurements and timing sessions a preliminary rider team was developed. PowerTap results can be seen in Table 1. Specific measurements were then taken from each of the riders so the vehicle could be designed around these dimensions. Designing the vehicle around the rider ensures a proper fit for the rider and produces a maximum efficiency for each rider. Through the rider measurements it was determined that each rider had fairly similar measurements and that adjustment during competition would be minimal. Rider measurements can be seen in Table 2.

Table 1: Power Output Results of Test Run 2

Rider	Max Power (Watt)	Average Power (Watt)	Max Speed (MPH)	Average Speed (MPH)	Average Cadence (RPM)	Energy Expenditure (Kilojoules)	Distance (Miles)
Maurycy Sarosiek	655	364	24.1	15.0	56	26	0.32
Jesse Cordero	423	242	19.2	12.7	48	21	0.20
Mike Studer	636	194	17.4	10.7	40	17	0.28
Jonathan Incorvaia	625	314	20.2	13.2	54	24	0.29
Sepideh Norouzi	Data Did Not Record						

Table 2: Primary and Back-Up Rider Measurements (all measurements in millimeters)

Rider	Height	Foot to Hip	Foot to Knee Cap	Torso Height	Shoulder Width
Jonathan Incorvaia	1702	914	508	787	483
Mike Studer	1727	965	559	762	457
Ray Palomino	1727	991	533	737	483
Dave Walker	1727	965	559	762	457
Maurycy Sarosiek	1702	991	457	711	457
Jesse Cordero	1676	1016	483	660	457
Sepideh Norouzi	1676	991	533	686	381
Average	1708	978	514	730	454
Maximum	1727	1016	559	787	483
Minimum	1676	914	457	660	381

Design Description

The goal of this year’s HPV team was to design a vehicle that was practical and easy to use yet still obtain high performance. The team first evaluated previous vehicles built by Matador PedalSports as well as top performing human powered vehicles from the past five years of the HPVC. Through identifying each vehicle’s strengths and weaknesses the team could then compile a design matrix and establish which design features were more important. The team was separated into individual departments: Frame and Structural, Aerodynamics, Materials Testing and Safety, System Integration, and Administration and Finance. Each design department was responsible for their respective aspect of the design, except for System Integration. The specific task of the system integration department was to ensure a cohesive design, they checked for clearance issues, certain part requirements, overall they ensured everything would come together correctly. A

preliminary design matrix and detailed design matrix can be seen in Tables 3 and 4 respectively. It can be seen through Tables 3 and 4 that the selected configuration of the human powered vehicle is a tadpole recumbent tricycle with front wheel steering, rear wheel drive, and front wheels placed outside the fairing. From the design matrices a more detailed design description was developed through multiple design meetings. Once the overall configuration was decided each department in the team organization proceeded to compile a detailed design of the vehicle components in their area of responsibility. Weekly design meetings were held between all department lead engineers to ensure a cohesive design process.

Table 3: Preliminary Design Matrix (scale: 1 to 3, 3 being best)

	Stability	Safety	Ride ability	Aerodynamics	Totals
3-Wheel Recumbent	3	2	3	2	10
2-Wheel Recumbent	1	1	1	3	6
2-Wheel Upright	2	3	2	1	8

Table 4: Detailed Design Matrix (scale 1 to 2, 2 being best)

	Complexity	Weight	Manufacturability	Reliability	Stability	Aerodynamics	Totals
Rear Steering	1	1	1	1	1	2	7
Front Steering	2	2	2	2	2	1	11
Rear Wheel Drive	2	2	2	2	1	2	11
Front Wheel Drive	1	1	1	1	1	1	6
Full Fairing	1	1	1	1	1	2	7
Wheels Outside Fairing	1	2	2	1	1	1	8

Through the design matrices and team member research the optimal structural platform was determined to be a structural belly pan made from an aramid honeycomb core sandwiched between layers of carbon fiber composites. The aramid honeycomb core provides the compressive strength needed that the carbon fiber lacks. The structural belly pan provided many design options. It provided a single flat mounting platform for attaching all components. This aids in allowing variations of design, i.e. a vehicle more geared for safety rather than speed, or a vehicle that can carry a small package. The structural belly pan also aids in ease of manufacturing, since a flat sandwiched core can be manufactured fairly easily and quickly.

The next portion of the vehicle to be designed was the drive train. This is one of the most important aspects of the vehicle. The drive train needs to be simple, efficient, and reliable. If the chain is not aligned properly it will constantly fall off the sprocket. To eliminate losses due to chain tensioners the drive train department decided to use a multi-chain drive train. Figure 2 shows the drive train layout. Chain 1,

highlighted in red, travels from the crankset to the transfer gear under the rider's seat. Chain 2, highlighted in green, travels from the opposite side of the transfer gear hub to the rear wheel. The primary component of the drive train is the crank set and bottom bracket bearing assembly. In recent years a new technology for bottom brackets has arrived. The BB30 bottom bracket is the cycling industries leading bottom bracket. The BB30 eliminates the need for bottom bracket bearing cups. The cups add complexity in manufacturing and a small amount of weight to the vehicle. The greatest advantage to BB30 technology is a much stiffer crankset, which minimizes losses due to deflection. These losses decrease the efficiency of the rider to transfer all of their power through the pedals to the drive wheel. From the available options of BB30 cranksets, the SRAM Red crankset was chosen for its light weight and race applications. Chaining sizes were determined after the transfer gear hub was chosen (described below).

The crank mount size was determined by the arm length of the crank and the size of the largest foot from the team of riders. From a crank arm length of 172.5 mm, adding 150 mm for a foot clearance the height of the crank mount was determined to be 322.5 mm to the center point of the bottom bracket. The general shape of the mount is a triangular upright to evenly distribute the forces through the entire part. The width of the crank mount is dictated by the width of the bottom bracket, 68 mm. The team manufactured an aluminum crank mount that uses a clamping system to hold the bottom bracket in place. The bottom bracket will be experiencing mainly rotational forces; therefore the clamping force required will be minimal.

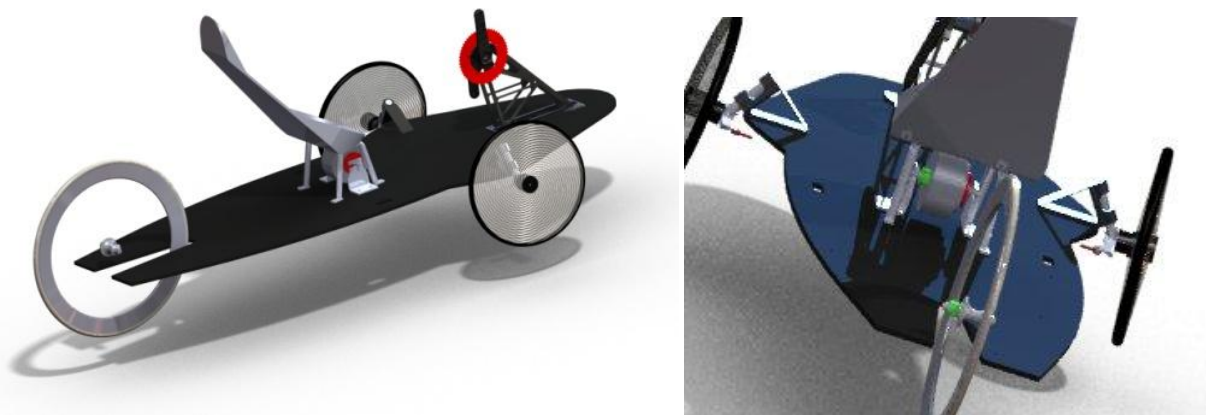


Figure 2: Drive train layout

From the crankset the chain travels under the seat to the transfer gear. The decision to use a transfer gear was based on several factors. An initial issue arose when designing the drive train of how to mount a traditional chain derailleur. Traditionally a derailleur mounts on the outside of the rear wheel drop-outs. With the belly pan design the structure of the belly pan interferes with that mounting. To alleviate that issue the use of an internally geared hub was the best option. Since internally geared hubs are typically heavier than traditional gear sets the hub was moved under the rider's seat. Doing so reduced the inertia of the rear wheel. To determine what effect, if any a rotating mass would have on the vehicle a comparison between the rotating mass of a rear wheel and the rotating mass of the transfer hub was completed. The equation used can be seen in Equation 1. Through the comparison it can be seen that a wheel with a mass of 0.226 kg would be needed to have an equivalent rotational inertia as the internally geared hub. Since all wheels are much heavier than 0.226 kg this tells us that the rotational inertia of the internally geared hub is much less than the inertia of the wheel and is thus of no consequence. The transfer gear hub is mounted with simple brackets machined from 6061-T6 aluminum.

Equation 1: Rotational Inertia $I = m(r^2)$

The transfer gear also reduces the risk of losing a chain. Since all the shifting is done inside, the chain stays on the same sprocket no matter what gear it is in. In addition to a smoother shifting process the internally geared hub eliminates the need for idler gears or chain tensioners. Idler gears and chain tensioners are inherently faulty. They seize very easily under high performance conditions and introduce friction losses into the drive train. Using an internally geared transfer hub also allowed us to use an extremely light and aerodynamic rear track wheel. The transfer gear hub chosen is a NuVinci CVP, a continuously variable planetary, internally geared hub. The hub gives the vehicle a gear range of 350%; using that gear range the front chainrings were chosen. Every gear throughout the vehicle, except for the chainrings, is an 18 tooth gear; the chainrings were chosen to be 53 and 39 teeth. The vehicle's top speed was calculated assuming a crank RPM of 100 (average human cadence) to be: 71.9 kph (44.7 mph) with a 53 tooth chainring, and 52.9 kph (32.9 mph) with a 39 tooth chainring.

Deceleration of the vehicle is just as important as acceleration. Human powered vehicles are much smaller than cars yet share the same roads, and sometimes lanes. The HPV is at a huge safety disadvantage compared to a car. In the event of a collision with a car the rider could be seriously injured as well the HPV could be destroyed. The braking system of the HPV is one feature that greatly adds to the overall safety of the vehicle. We are using hydraulic disc brake assemblies in the front and a caliper brake in the rear. The main portion of the braking system will be the front disc brakes, they are designed for downhill mountain biking. Vehicle speeds in downhill mountain biking are less than those in road use but the bicycles are heavier and the slope of the hill comes into greater affect. Therefore the disc brakes will provide ample braking force. To simplify the braking system for the front wheels the hydraulic lines will be spliced together and will therefore only require one lever. The rear brake caliper will mount directly to the belly pan using a potted insert (seen in Figure 16).

After the gearing was established the wheel supports were designed. Through the design matrices mentioned above the wheel locations were already determined; the manner in which they were fastened to the vehicle was not. The rear wheel is mounted to an "L" bracket on the rear edge of the belly pan. The horizontal portion of the bracket is supported by the rear stay of the roll bar as well. There is a slot for the rear wheel hub to mount into to allow the chain to be tensioned during final assembly.

The front wheel mounts are more complex and went through multiple iterations. The wheel axles, referred to as kingpins, are very complex to manufacture and are an integral support for the vehicle. Therefore the kingpins were purchased from Catrike, a reputable recumbent tricycle manufacturer. The kingpins must be mounted onto the belly pan. The first iteration was a simple "pipe flange" arrangement. Through Finite Element Analysis (FEA) the pipe flange kingpin holders were determined to be insufficient. The second and final iteration was a triangular bracket that securely mounts to the belly pan. The FEA analysis performed on the kingpin holders placed an offset 5G upward force through the holder to simulate an impact from a pothole. The results produced a safety factor of 7.3 and a maximum deflection of 0.06 mm. The kingpin holder can be seen in Figure 3.

The wheels to be used are standard 20" wheels in the front and a 700mm track wheel in the rear. The rear wheel is a track wheel due to the fact that the chain will be running on the traditionally non-drive side of

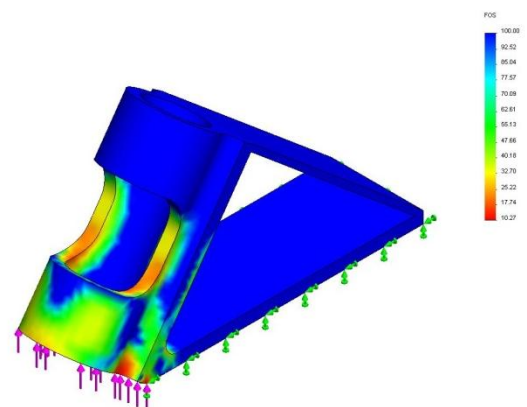


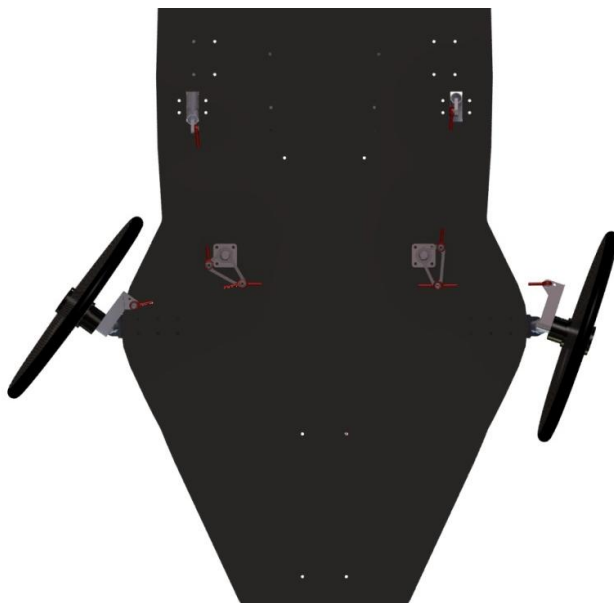
Figure 3: Stress Distribution for Kingpin Holder

the vehicle. A track wheel is a fixed gear hub and can run in either direction. Additionally the track wheel has a very low rolling resistance and is designed to be very aerodynamically efficient.

Once the drive train layout was complete, design of the seat, steering assembly, and rollover protection system was finalized. Location of the seat relative to the crankset was determined through measurements taken by the biomechanics department. The seat location was placed at a position to optimize the rider's leg stroke. According to research in cycling dynamics textbooks, an optimal stroke is one that does not fully extend the leg; the knee must be slightly bent at maximum extension. [2] In addition to leg extension, seat back angle is also important. Based on rider measurements and recumbent cycling research a seat back angle of 50° from vertical was used to optimize the rider's leg force to the pedals. The seat is supported by two "U" shaped 7/8" aluminum tubes that mount flush to the belly pan. Both seat supports are joined together by a small cross piece of aluminum that the seat will mount directly to. Once the seat location and angle were determined the location of the steering assembly and handlebars were determined.

The steering system is a very critical component of the vehicle for obvious reasons and because of its importance many different designs were considered to determine the ideal configuration. Different configurations that were analyzed included the cross bar design, bell crank design and inverted bell crank design. The cross bar design was the legacy design from a previous CSUN recumbent vehicle, and was analyzed and determined to be fundamentally problematic with the current vehicle configuration. This design had crossbars that crossed directly between the seat and the pedals, directly interfering with the chain as it passed towards the drive wheel. Several suggestions and design considerations were made to try and route the chain around the crossbars but simplicity and reliability of the system would have been compromised if these changes were made. Because of the drawbacks discovered with the crossbar design this configuration was abandoned. The next design that was considered was the bell crank configuration. This design eliminated the interference with the chain that the crossbar design encountered because the bell crank uses two parallel rods to transfer the motion from the steering device to the bell cranks on either side of the chain. The problem that was discovered was the possibility of the rider's feet hitting the bar connecting the two bell cranks together. The possibility of kicking the steering system was a huge drawback that led to the third and final design, the inverted bell crank.

The inverted bell crank is essentially the bell crank design discussed above, but put on the underside of the belly pan in order to protect all of the steering bars from interfering with both the rider and the chain.



This design was both simple and reliable because there is no possibility of interference. The inverted bell crank does have the possibility of ground interference when traveling across a slope, but this problem was evaluated and determined not to be a problem because of the position of the bell cranks relative to the front wheels. This design is ideal because it allows adjustability of the required driver input in order to fine-tune the feel of the steering system. Thus the inverted bell crank design was determined to be the best suited configuration for the vehicle. The inverted bell crank steering system can be seen in Figure 4.

Figure 4: Inverted Bell Crank Steering System

The steering system also employs an innovative feature in tadpole recumbent design known as Ackermann steering. The Ackermann steering system allows for the front wheels to be in an active camber situation. This means as the wheels turn the camber increases to achieve a smaller turning radius. They also contain corrective caster. The caster angle in wheels is defined by the angular displacement from the vertical axis of the kingpin. Caster allows the wheels to “auto correct” themselves. The combination of the Ackermann steering and corrective caster creates a much more responsive, accurate, and efficient steering system. [1]

Based on the seat back angle and torso height of each rider listed in Table 2 the effective height of the roll-over protection (roll bar) could be designed. In the event of a roll-over the roll bar must be tall enough to provide head protection for the tallest rider, wearing a helmet. In addition to a top impact the roll bar must also provide side protection to the rider. Thus, the roll bar must be outside the widest rider’s shoulders. According to the rules set forth by ASME the roll bar must protect the rider through two specific loading scenarios: a 600 lb, 272.15 kg top load directed 12° from vertical towards the rear, and a 300 lb, 136 kg side load directly horizontal at shoulder height. Through each loading scenario the roll bar must deflect no more than 2 inches. To ensure the safety of the rider and compliance to the rules the roll bar was designed using SolidWorks and analyzed with Simulation (FEA). Through several iterations to reduce weight yet adhere to the specific design constraints, a final roll bar design was completed. From the FEA analysis the final weight of the roll bar is 2.4 kg; it has a factor of safety of 2.55 and a maximum displacement of 16mm (.63 inches) for the top safety load condition and has a factor of safety of 1.6 and a maximum displacement of 11mm (.43 inches) for the side load safety condition. The final roll bar design as well as FEA analysis plots can be seen in Figure 5a and 5b. The vehicle will also include a commercially available 4-point safety harness that will mount to the cross bar of the roll bar as well as the aluminum seat mount and will hold the rider inside the vehicle in the event of a roll-over.

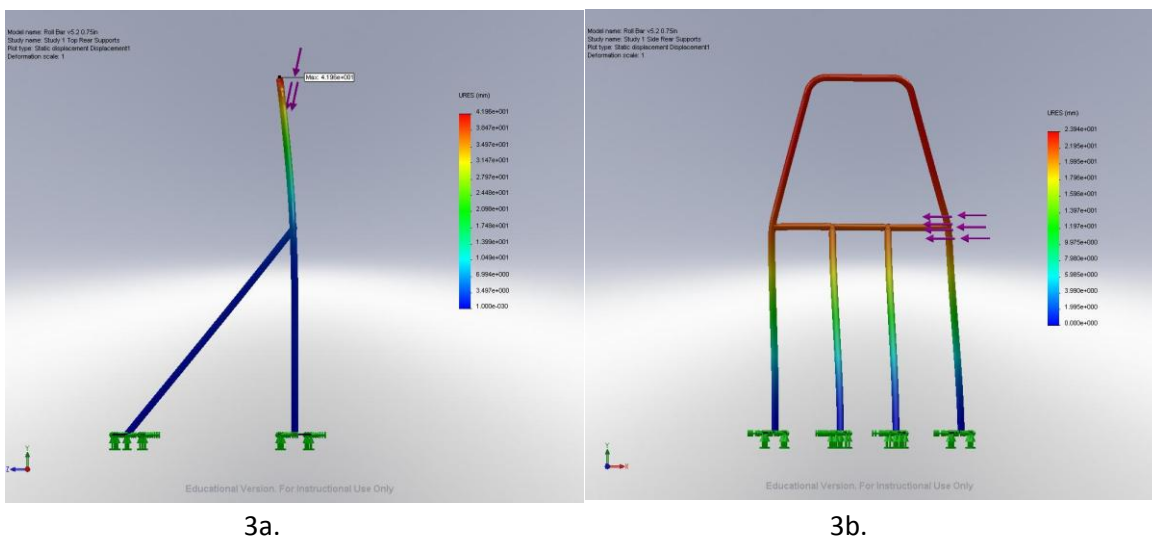


Figure 3: Final roll bar design with FEA analysis: 3a: Top load with maximum deflection; 3b: Side load with maximum deflection.

Throughout the entire design process, aerodynamics of the vehicle was considered. Once the general shape of the belly pan was defined, the aerodynamics department began to design the fairing. To reduce the aerodynamic drag the vehicle is enclosed with a 3/4 fairing. The fairing covers the body of the rider, while

leaving the driver's head exposed to the air. Since the front wheels and their associated structure are slender and will produce minimal drag at the design speed of the vehicle, they were not covered by the fairing. This decision allowed the use of a narrow teardrop shape for the fairing. The streamlined shape of the fairing should limit the amount of stagnation points and by that ensures maximum efficiency of the vehicle.

Although aerodynamics was of primary concern, rider's comfort and visibility were also of a significant importance to the aerodynamics department. Visibility and ease of manufacturing were the determining factors in leaving the head of the rider exposed to the air. The fairing is also designed to ensure ease of access. The access to the vehicle will be done through a large hatch that will provide for an easy and fast way to exit and enter the vehicle.

The first step in manufacturing the fairing molds was to create a mock-up of the fairing. The mock-up was designed to optimize the size of the fairing while giving adequate clearance for all of the riders. It was constructed by using cardboard, wood, glue, some bolts and screws, and an upright crank. For this pre-manufacturing step, a wooden frame was created to hold cardboard cutouts of the fairing cross sections. Only selected areas that were critical to the rider function within the fairing were cut out and placed onto the mock-up. Those cross sectional pieces were then placed onto the wooden frame at their proper measurements (See Figure 6a). Seat and crank set-ups were also included within the space so that the rider could actually get in and try out the space within the mock-up. The tallest rider checked the space for clearance (see Figure 6b). Knee, toe and shoulder clearances were verified before the manufacturing process began. Adjustments were made accordingly to ensure comfort and optimum performance. The mock-up had a length of 2512.8 mm, a width of 711.9 mm, seat location of 1227.1 mm from the front of the fairing, and a crank set-up location of 436.6 mm from the front of the fairing.



Figure 6a: Mock-up of Fairing Space



Figure 6b: Tallest Rider

After adjustments were made on the mock-up, the changes were implemented in the SolidWorks model. Originally, the male mold was going to be created in one whole piece using a skeleton and skin method. To save time and gain accuracy it was decided to machine the fairing mold in a professional machine shop. Since the machining tool required a minimum height of 762 mm, it was decided to make the mold in 6 sections. Each section met the required height. Figure 7 shows the respective sections.

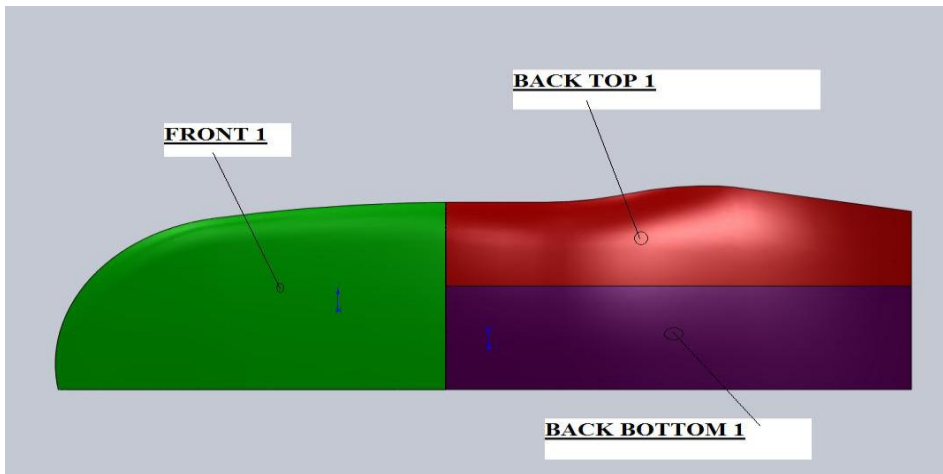


Figure 7: Side View of the Section



Figure 8: Stacked Foam

After the size of the sections was determined the adhesives required to hold the foam sheets in large sections was researched through sample testing of excess foam. Heavy duty construction adhesive was determined to be the optimal adhesive to hold the pieces together. Figure 8 illustrates the form at which the foam was sent to the machine shop. The next step was to build a tool that would hold the sections of the fairing in place while machining is taking place. The tool was made out of 1" thick flat plywood with wooden pins attached to it. There were two tools created in a size of 812.8 mm by 1193.8 mm and the other in 431.8 mm by 1422.4 mm. The tools were used to hold the foam stacks down so that the machines could cut out the contours of each stack in one setup. Figure 9 shows the SolidWorks model of the tool and the front section of the fairing.

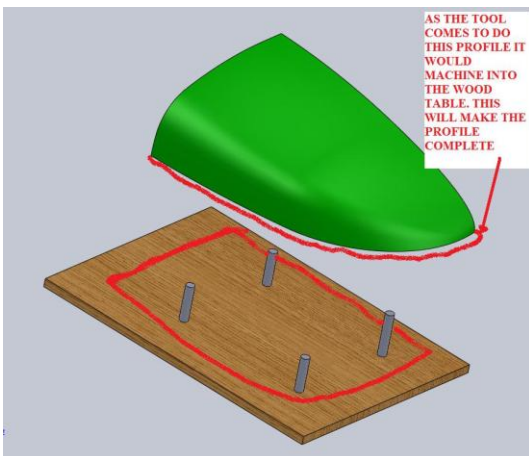


Figure 9: Tool Used to Hold Foam During Machining Process

fairing.

The ease of entry and exit from the vehicle is an important topic in the fairing design. From previous experience it is known that for the speed endurance event considerable amount of time is lost during rider exchange.

Although the fairing has an open cut for the rider's head, the opening is not wide enough for the rider to merely jump in and out of comfortably. For this reason the fairing will incorporate a hatch. The hatch will be incorporated into the fairing so that the rider will be able to enter and exit the vehicle without assistance, thus minimizing entry and exit time and improving safety. The hatch will open over the length of the vehicle and will be hinged on the side to allow the rider to open it without assistance. Figure 10

illustrates the location and orientation of the hatch; the blue line represents the area the hatch will be cut from. Along the seam of the fairing there will be exposed sharp edges and possibilities of mismatch between

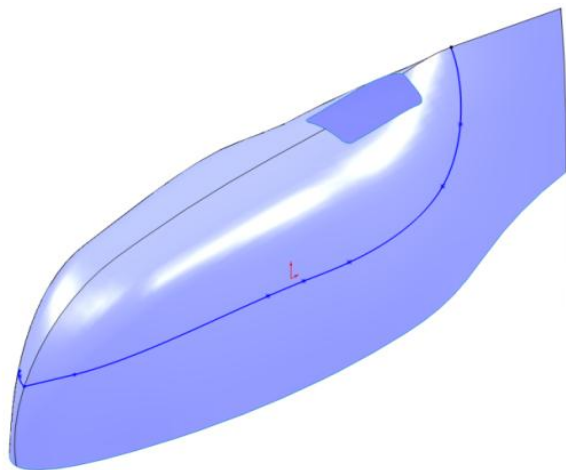


Figure 10: Fairing Hatch for Entry and Exit



Figure 11: Moroso Quick Release Fasteners

the mating components, so the mating surfaces will be covered with weather stripping. These strips will protect the rider from sharp edges and also stop air from entering the vehicle.

A problematic area of years gone by has been the fastening methods for the fairing pieces. On some occasions in the past the CSUN HPV team has suffered with unreliability in regards to the fairing mounting. Poor attachment methods have led to fairings falling off in mid-competition, also fastening methods were neglected until the fairing was designed and built. The neglect led to “Mickey-Mouse” attachment methods, which in turn ended up hurting the final aerodynamics of the vehicle.

The aerodynamics department will utilize attachments that will be permanent when needed, and will provide minimum fairing deflection as not to affect the performance of the vehicle.

The main attachment points for the fairing are along the periphery of the belly pan frame. The method to be used to attach the fairing to the frame will incorporate quick release fasteners, small hinges and draw latches. The quick release fasteners will attach the complete fairing to the belly pan. They allow for fast and easy removal of the fairing for vehicle repairs or modifications; the only tool needed to release them is a flathead screwdriver (see Figure 11). The quick release fasteners are designed for use on race car panels; they are very easy to install and are highly efficient to use. To secure the hatch to the primary fairing we will be using multiple small hinges and a simple draw latch that can be operated with one hand. The quick release fasteners, hinges and latch will be placed on the interior of the fairing to ensure the integrity of the aerodynamics.

The exposed edges where the fairing pieces meet will be covered using weather seal strips. The weather seal strips will be used for multiple reasons, especially air flow and protection. The weather seals will ensure that the exposed surfaces will not allow air flow to be disrupted at intersecting edges. The secondary use of the weather strips is to protect the fairing from wear and tear as it is continuously moved around and mounted. The rules mention that the judges at the competition will be looking for sharp edges on the vehicle as part of the safety inspection. The weather seals will be an added safety feature in this regard, as it will cover the exposed edges of the fairing.

Materials Science and Testing

Material choice is a very important decision when building a human powered vehicle. A HPV is built for speed, acceleration, good handling characteristics as well as ease of ride for the speed endurance portion of the competition. A lighter vehicle will achieve a higher performance, particularly when decelerating and accelerating while negotiating corners. Different materials have their strengths and weaknesses, and an optimal balance has to be found between the material characteristics as well as the vehicle design criteria.

Table 5 lists some of the important properties of common materials. The specific tensile strength quantifies the strength to weight ratio of the material. Table 5 shows the significant advantages offered by aramid and carbon fibers over metals such as steel, aluminum, and even titanium.

Table 5: Material Properties

MATERIAL	DENSITY (g/cc)	TENSILE STRENGTH (ksi)	SPECIFIC TENSILE STRENGTH	TENSILE MODULUS (Msi)	SPECIFIC MODULUS
Steel	7.8	145	19	29	3.5
Titanium	4.5	134	30	16	3.5
Aluminum	2.8	67	24	10	3.5
Glass Fiber	2.5	246	98	10	4
Carbon Fiber	1.9	228	120	55	29
Aramid Fiber	1.4	385	275	19	14
Boron Fiber	2.6	443	170	23	9
SiC Fiber	3.5	500	143	57	16

Specific Modulus, which is a stiffness to weight ratio, is another very important material property. The frame system has to be stiff to allow for a maximum transfer of power from the rider to the crank/chain and down to the wheel/road. Even though carbon fiber is not the lightest material, its specific modulus is unmatched. It also possesses good tensile strength.

Steel and Aluminum are abundant, easy to manufacture, and inexpensive in comparison with many other candidates. Table 5 shows their properties and the reason for not using them is clear. Density and specific modulus are not favorable compared to the other materials. It would make the vehicle very heavy to account for the shortcomings of their properties and in effect significantly lower the performance. The advantages of ease of manufacture and low cost do not justify the large decrease in performance. Yet another big advantage of composite materials over metals is the fatigue strength. The composites exhibit a six-fold improvement over metals in the 10^6 to 10^8 cycle range. It can be seen clearly that composite materials, specifically carbon fiber, is a desired material for manufacturing a human powered vehicle. Overcoming its disadvantages of complex manufacturing with long cure times, high cost and extensive analysis required will be rewarded with a light and strong vehicle ready for the competition.

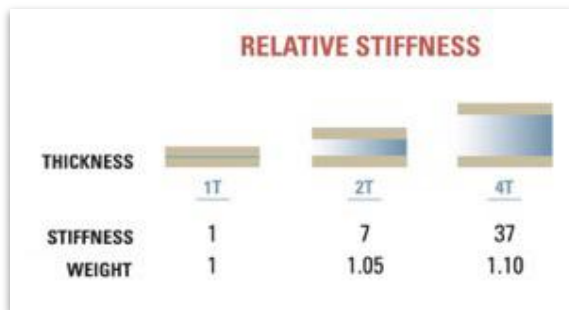


Figure 12: Relative Stiffness

The frame of our HPV incorporates a honeycomb construction. It gives the necessary stiffness with marginal weight increase with respect to the thickness of the honeycomb core. As shown in Figure 12, doubling the core thickness increases the stiffness seven times while the weight only increases by 5%. The stiffness ratio keeps increasing significantly with the core thickness.

Having a strong light weight material as a core is a key feature to keep the amount of top and bottom material to a minimum. The core will take care of compressive strength and the carbon fibers will dominate tensile strength properties for the frame.

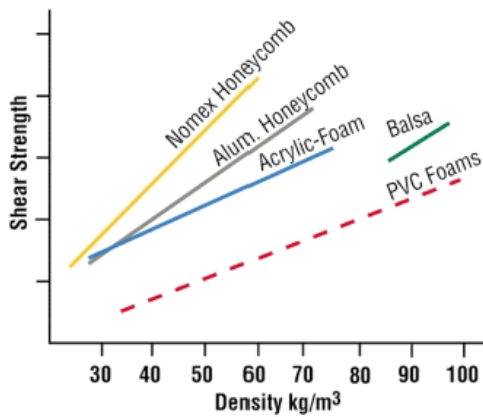


Figure 13: Core Shear Strength vs. Density

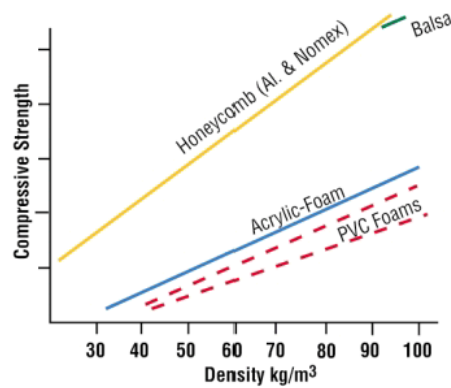


Figure 14: Core Compressive Strength vs. Density

Nomex honeycomb is the core of choice due to its key properties. As shown in Figure 13 nomex's shear strength versus density exceeds all of the other candidates. In Figure 14 it is comparable with aluminum core on the compressive strength versus density. This shows that we can have a lighter core and hence lighter vehicle achieving similar properties. Another advantage of nomex honeycomb core over aluminum honeycomb core is that it is easier to work with when it comes to cutting holes and trimming to size.

Another material used in construction of this HPV is G10-FR4 Fiberglass. High compressive forces will be acting on the belly pan due to different attachments such as the steering mechanism, suspension, roll bar, etc. Fiberglass sheets are used as hard points for all of these attachment locations. Its compressive strength reaches up to 413.7 MPa where the honeycomb can only handle up to 3.4 MPa.

The process in which carbon fiber products are manufactured is just as important as its material properties. The flat belly pan was constructed by sandwiching the honeycomb core between layers of carbon fiber in one complete lay-up process. Complete saturation of carbon fiber fabric is very important as too little or too much resin will actually weaken the structure. Carbon fiber was unrolled from the roll onto a bagging material without cutting it and resin was poured on top of it in the middle. Another piece of bag was placed on top of it and the resin was moved around through that top bag with a squeegee. By doing so the fibers are not being pulled on directly and their orientation can be preserved for optimum strength in a given direction. Spreading the resin from the center out allowed for removal of the excess out through the edges and ensured even saturation. Once this was done the carbon fiber was cut with shears and since the fibers were stuck together they did not fray. One side of the bagging material was removed and a carbon fiber piece was laid on the layup with desired orientation. Once in place the other side of the bag was removed and another piece of carbon fiber was laid on top of it and so on. The size of the belly pan allowed for pieces of about 1.2 x 0.61 meters to be prepared at a time. Overlap of such pieces was 6.35 mm. This method allowed for faster layups with great precision and accuracy.

The top layup consists of four layers of plain weave (PW) carbon fiber in the orientation of 0, 90; 45, -45; 45, -45; and 0, 90 degrees with respect to the back of the vehicle. It also had about 12.7 mm overlap over the honeycomb. Layer of peel-ply and breather were placed on top and the whole belly pan was vacuumed bagged. Table 6 shows the complete carbon fiber and honeycomb lay-up.

The core material used was .5 inch thick nomex honeycomb having 1/8 inch cells with 3 per cubic foot density. Prior to lay-up the honeycomb was cut to the exact size of the vehicle shape and fiberglass inserts

were placed into the belly pan. These inserts were 6.35 mm oversized in relation to the mounting surface of the respective components. They were bonded to the honeycomb with the use of thickened epoxy mixed with microspheres and graphite balls which increase its toughness. Once this was done the core was laid on top of the bottom layup which was up to 12.7 mm larger than the finished frame to ensure complete coverage of the honeycomb.

The bottom layup consists of four full layers of carbon fiber and a few extra strips in key areas to strengthen the frame. Starting from the bottom, the first layer was plain weave carbon fiber with the orientation of 0, 90 degrees with the rear of the vehicle establishing a reference axis. It will be laid on top of the MDF (medium density fiberboard) plywood sheet with a laminate top surface which was treated with mold release spray. Following were strips of uni-directional (UNI) carbon fiber between the front suspension and other key areas. The next three layers were laid out of UNI in the orientation of -45, -45 and 0 degrees. This concluded the bottom layup of the belly pan upon which core material was placed.

Table 6: Lay-Up schedule from Top surface downward

Ply	Orientation
Plain Weave Carbon Fiber	0°, 90°
Plain Weave Carbon Fiber	-45°, 45°
Plain Weave Carbon Fiber	-45°, 45°
Plain Weave Carbon Fiber	0°, 90°
Nomex Honeycomb Material	N/A
Uni-directional Carbon Fiber	0°
Uni-directional Carbon Fiber	45°
Uni-directional Carbon Fiber	-45°
Plain Weave Carbon Fiber	0°, 90°

Once cured, the excess of bottom and top carbon fiber layup was trimmed off with a carbon fiber cut off wheel and the exposed honeycomb was closed off with 50.8 mm wide PW carbon fiber tape. This fully enclosed the nomex core and eliminated any sharp edges.

The fairing of the vehicle is going to follow the same lay-up process as the belly pan of the frame, where the layers of fabric will get squeegeed to disperse the amount of resin evenly throughout. Because the fairing has a larger surface area, the number of layers is going to be as few as possible so that it can reduce weight while still providing rider protection in the case of a rollover.

The base layer, the one closest to the rider, will be plain weave carbon fiber oriented at 0, 90 degrees referenced from front to back of the fairing. The next layer will be of Kevlar. Because Kevlar behaves strongest in the axial direction as opposed to the transverse direction, it will be layered accordingly. Kevlar is going to be used because of its high modulus strength as well as tensile strength, but its main purpose in our application is going to be puncture and abrasion resistance in the rare case that a rider happens to crash into an obstacle. The last layer of fiber will be another layer of plain weave oriented at 45, -45 degrees from the front to the rear starting at the bottom drive side as a reference to plane angle direction. Kevlar isn't as moisture resistant as carbon fiber which is one reason that it is going to be sandwiched in between the two carbon fiber layers. In addition UV light degrades Kevlar; the layers of carbon fiber on either side of the Kevlar will protect it from UV light. Also it will help prevent delaminating. Due to the large size of the fairing the material will have to be laid up in several pieces for every layer. A 6.35 mm overlap for each sheet will be made in order to maintain the strength and integrity.

The resin was chosen accordingly to the design of the layup. Something with good coverage/volume ratio as well as slow curing and low viscosity was necessary because there was going to be a honeycomb core and several layups of plain weave and uni-directional carbon fiber. The resin of choice was the Pro-Set 125 resin and 225 hardener combination. The 125 resin is a low viscosity resin that provides fast and thorough wetting of the laminate fibers. Because it was also used in the 2008-2009 HPV team vehicle, we know that when cured it provided a greater fiber to resin ratio and was ideal for working with the thicker weaves. The 225 hardener was chosen due to its longer pot life (approximately 77 min) when mixed with the 125 resin. Even though there is no post cure required for this combination, we will be doing so in order to achieve the highest possible properties for the material. This combination of resin and hardener can provide approximately 160 min of working time at 72°F and gel time begins around 5 hours after.

Table 7: Properties for Pro Set 125/229 mix at room temp and post cure

<u>Properties</u>	<u>Curing at Room temperature after 2 weeks</u>	<u>Curing at 72°F for 15 hr + post cure @ 60°C for 8 hrs</u>
Compression Yield (MPa)	100	101.5
Tensile Strength (MPa)	52	70.65
Tensile % elongation	3.5	4.05
Flexural Strength (MPa)	89.4	121.5

As seen in Table 7, the property values increase significantly with the addition of a post cure process. The biggest values that helped make our decision about using a post cure method were the tensile strength increase from 52 MPa to 70.65 MPa as well as the flexural strength that jumped from 89.4 MPa to 121.5 MPa. These higher values will help eliminate any second guessing on the fatigue of our belly pan structure as well as any last minute repairs before the race.

Potted inserts will be used in non-load bearing locations such as the steering rod locations and bell crank locations. They will need to be incorporated into the belly pan by means of conventional milling or drilling the root diameters into the belly pan. These pilot holes will need to range from 0.127 to 0.254 mm bigger to allow for shrinkage as well as a gap for bonding. Aluminum will begin to corrode when joined with other dissimilar material hence as seen in Figure 15 a layer of fiber glass will be incorporated along with the bonding epoxy to help reduce galvanic corrosion.

The pilot holes will weaken the integrity of the carbon fiber layups, however, counter balance of the loss of physical properties will be made with inserts that will absorb some of the stress as well as distribute it over a large area of carbon fiber. Oversize flanges on the top and bottom of the inserts shown in Figure 15 will

distribute bending as well as tensile stress on the frame eliminating point loads.

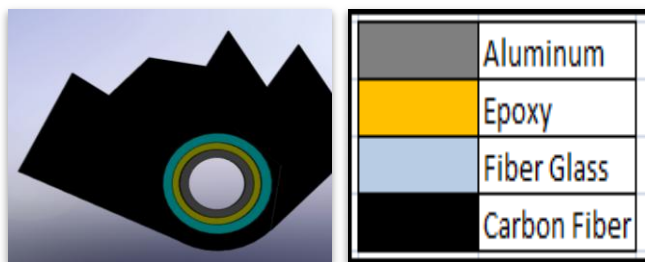


Figure 15: Detail of Potted Insert

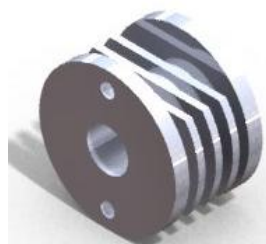


Figure 16: Aluminum Potted Insert

The adhesive for bonding inserts in the belly pan will be Pro-Set 175/277. This adhesive provides great shear and peel adhesion, and 20 min work life. Its tensile strength is approximately 41.3 MPa with tensile adhesion to 2024 Aluminum being approximately 13.8 MPa. Besides its desirable properties, cost is of concern as well. The Pro-Set adhesive is affordable with a price tag of about \$80 per pint. 3M-DP420 will be used in some areas due to its superior properties but the cost is about 400% higher. This adhesive will be used as a primary applicator for many of the add-ons to the main belly pan structure, where fiber wraps around the adhered part will then be applied to strengthen the bond.

Design Analysis

A vehicle's center of gravity has a strong effect on the cornering stability. The center of gravity of the vehicle (without the rider) was taken from the mass properties in Solid Works. Once the center of gravity was obtained (in terms of the x, y, and z coordinate), the results went into the overall center of gravity calculation for the vehicle including the rider. As seen in Table 8, the new center of gravity was obtained and by using those results the weight distribution on the front wheels and back wheels were obtained. Using the results in Table 8 and assuming a 4.5 meter radius corner, the rollover was calculated in Table 9.

Table 8: Center of Gravity Calculation

Weight Inputs:			
19.1	<-- Wv, vehicle weight (kg)		
81.6	<-- Wp, weight of person (kg)		
Center of Gravity Inputs:			
630.4	<--CGx, vehicle center of Gravity from front wheel (mm)		
304.8	<-- CGz, vehicle center of Gravity from the ground (mm)		
609.6	<-- d1, CGx-distance from front wheel to Rider (mm)		
406.4	<-- d2, CGz-distance to Rider from floor (mm)		
1478.3	<-- l, distance from front to back wheel (mm)		
Center Gravity Outputs:			
Equations:			
$Wt = Wv + Wp$	Total weight, Wt -->	100.7	kg
$W\% = (CGx/l) * 100$	Weight distribution on the front wheel, W% -->	42.6	%
$CGxvp = (Wv * CGx + Wp * d1) / (Wv + Wp)$	Center of Gravity on the vehicle & Person, CGxvp -->	613.5	mm
$CGzvp = (Wv * CGz + Wp * d2) / (Wv + Wp)$	Center of Gravity on the vehicle & Person, CGzvp -->	387.1	mm
$Wf = Wt * ((l - CGxvp) / l)$	Weight on the front wheels, Wf -->	58.9	kg
$Wr = Wt * ((l - CGxvp) / l)$	Weight on the rear wheel, Wr -->	41.8	kg

Table 9: Rollover Calculation

Weight Inputs:			
19.1	<-- Wv, vehicle weight (kg)		
81.6	<-- Wp, weight of person (kg)		
Center of Gravity Inputs:			
613.5	<-- CGxvp, Center of Gravity on the vehicle & Person (mm)		
387.1	<-- CGzvp, Center of Gravity on the vehicle & Person (mm)		
Speed Inputs:			
26.2	<-- V, vehicle speed (kilometers/hour)		
9.81	<-- g, gravity (m/s^2)		
4572	<-- r, radius of the curve (mm)		
914.4	<-- t, Track of front wheels (mm)		
Rollover Outputs:			
Equations:			
$Wt = Wv + Wp$	Total weight, Wt -->	100.7	kg
$a = (V * 1000 / 3600)^2 / (r / 1000)$	a, Lateral Acceleration -->	11.6	m/s^2
$F = (Wt * (V * 1000 / 3600)^2) / ((r / 1000) * g)$	F, Horizontal Lateral force -->	118.9	kg
$\theta = \tan^{-1}(CGzvp / (t / 2))$	vector angle, θ -->	40.3	°
$Fr = F * \tan \theta$	Resultant vertical Force, Fr -->	100.7	kg
$Wf = Wt * ((l - (l - CGxvp)) / l)$	Will the Vehicle Rollover -->	NO	
Note: When V was increased to 27 kph calculations dictated a vehicle rollover			

The analysis of the structural belly pan was crucial to the design of the vehicle. SolidWorks Simulation does not have the capability to perform FEA on carbon fiber composites so NEI-Nastran was used to perform the FEA of the belly pan. Prior to FEA calculations the material properties for each ply as well as the honeycomb core were defined. Through research and manufacturer technical data sheets values for each layer's strength, failure stress, shear stress, shear modulus, Young's Modulus, compressive failure stress, thermal expansion coefficient, Poisson's ratio, density, fiber thickness, percent (%) elongation, in plane shear modulus, and damping coefficient were input into the software package.

The loads were then placed on the belly-pan in their respective locations with the respective forces and directions positioned on the belly-pan accordingly using the software package, so that a static simulation on the belly-pan could be simulated. A 96.6 kg load was placed downward on the 4 bolt hole (fixture) locations for the seat, in order to simulate a 90.7 kg rider and also take into consideration the weight of the carbon-fiber seat at 5.9 kg. This load was then distributed evenly to each hole at 24.15 kg applied to each fixture point. A 39.4 kg upward load was then applied on to the rear two mounting brackets of the belly-pan that come off of the rear down-tubes of the roll bar. This load was then distributed evenly amongst the two set of bolt holes coming of the rear of the belly pan, with each mounting plate having three locations for affixing the plate to the belly pan per side. Thus 39.4 kg / 6 holes = 6.5 kg load applied to each rear hard-point with a fixed point defined in SolidWorks. The front wheel mounts and king-pin mounting locations were then used to apply another fixed point to the Nastran model with a 55.8 kg load that was placed in an upward direction upon the front two wheels, as pre-determined by the center of gravity and roll-over calculations.

This 55.8 kg load was then divided by 2 for the left and right wheels and again, divided by 6, for the six mounting locations (holes) that are going to affix the steering mounts and kingpins to the belly pan. Thus, after doing the math, the loads applied to each of the six holes on the front of the belly pan was entered into the Nastran as 4.65 kg per hole.

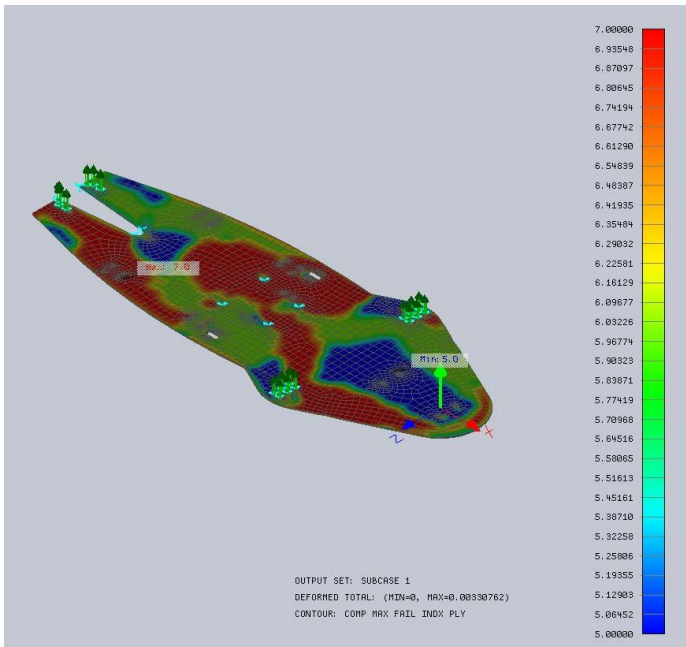


Figure 18: Factor of Safety Distribution

After all the loads were input a proper mesh was setup for both the top and bottom of the solid model of the belly pan in the Nastran simulation software with an element size defined as 1.25. Then mesh controls were applied to each bolt hole. Unfortunately we found out during our second trial run of the Nastran analysis on our model that the mesh control refinements were not compatible with our Nastran model and simulations run, as they continually caused errors in our analysis and forced the simulation run to crash once. Thus, it was determined that no mesh controls would be applied to the rather small holes drilled into the belly pan and used for fixture and loading points during the static simulation analysis of our composite belly pan. Through the FEA calculations the Factor of Safety (F.O.S.) determined by our analysis and is shown below in the detailed plot Figure 18. The F.O.S. was determined to range from a minimum of 5.0 at the blue locations seen in the Figure 18, generally seen towards the front of the belly pan, within the same general area as the crank mount and steering setup. Meanwhile a maximum F.O.S. of 7.0 as indicated by the red regions of the belly pan can be seen in Figure 18. Unfortunately, there is not a general or focused area for on the belly pan where the F.O.S. is either at its maximum or minimum value; instead it varies in an un-uniform fashion, as indicated by Figure 18.

general area as the crank mount and steering setup. Meanwhile a maximum F.O.S. of 7.0 as indicated by the red regions of the belly pan can be seen in Figure 18. Unfortunately, there is not a general or focused area for on the belly pan where the F.O.S. is either at its maximum or minimum value; instead it varies in an un-uniform fashion, as indicated by Figure 18.

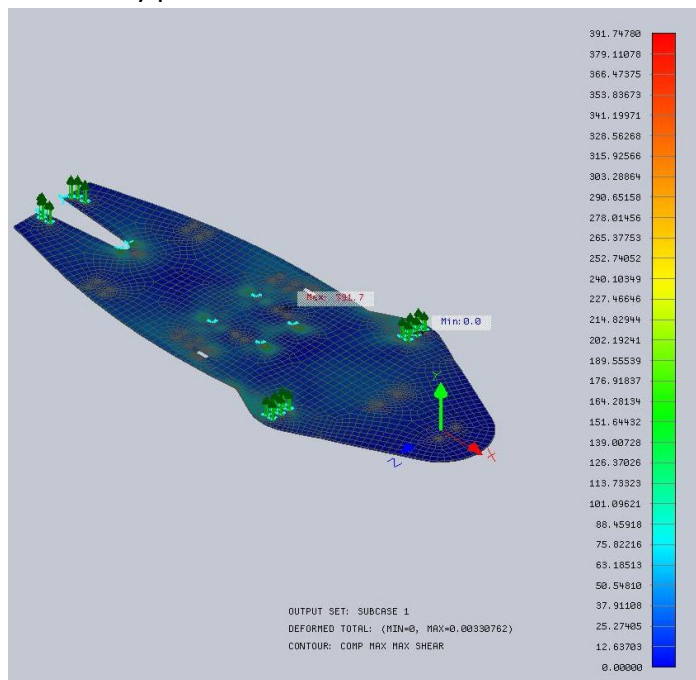


Figure 19: Maximum Shear Stress

Since shear strength is of concern the max shear stress was calculated as well. The maximum shear stress results shown in Figure 19 show areas where there is the increased potential for shear stress to occur as outlined by the green and yellow areas highlighted on our composite belly pan below. Again, the area of major concern seems to be located around the four mounting holes of the seat, where a maximum compressive shear stress result was given to be 2.7 MPa. The areas of the front wheel mounts, rear brake caliper mount, and rear down tube mounting surfaces are prone to experiencing shear stresses in the range of 0.6 – 1.03 MPa.

Displacement results for the composite belly pan analysis conducted using the NEI-Nastran software is shown below in Figure 20. According to

the displacement plot shown below in Figure 20, the displacement for the composite belly pan is at its maximum value of 0.078 mm and decreases in a circular radial fashion outward. If this analysis holds to be true and correct, then our belly pan will not experience much, if any deflection. However, if there is any deflection, bowing or displacement of the belly pan to take place, the first noticeable area where it will occur will again be under the seat of the rider, located at the geometric and theoretical center of the belly pan.

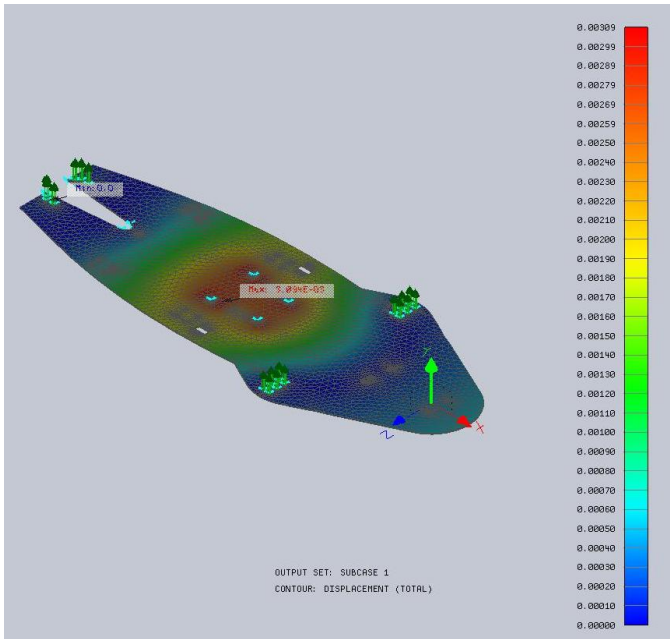


Figure 20: Maximum Displacement

Along with computer analysis physical testing on the composite material was done per the standard published by the American Society for Material Testing (ASTM D7249/D 7249M- 06). The scope of this standard covers the methods for testing the face properties of sandwich construction. The team was particularly interested in finding the flexural stress produced during the compression of the test samples.

The team chose to perform two loading configurations on the specimens (3-point and 4-point bending). We first performed a 3-point bending test to analyze the behavior of the material when the stress is localized over a small area; Table 10 shows the composition of the test specimens. Table 11 shows a description of the abbreviations used in construction and testing of specimens. For last year’s HPV, extensive tensile testing of carbon fiber samples was performed.

Based on previous data and the use of the exact same material, same manufacturer, fabric weight, resin, and manufacturing process, we have concluded that tensile testing would produce similar results and was therefore unnecessary.

Table 10: Test Specimen Lay-up and Identification

Sample ID	Top layup	Bottom layup	Core (in)
2 (A, B, C, D)	PW, 0, 90°	UNI 0°	0.5
	PW, 45-45°	PW, 45-45°	
	PW, 45-45°	PW, 0, 90°	
3 (A, B)	PW, 0, 90°	UNI 0°	0.5
	PW, 45-45°	UNI 45°	
	PW, 45-45°	UNI -45	
		PW 0, 90	
2 X 2	PW, 0, 90°	PW, 45-45°	0.75
	PW, 45-45°	PW, 0, 90°	



Figure 21: Typical Bottom Layup of Samples with Identification

The top layers of the samples were kept constant. The team concentrated on varying the configurations of the bottom layers since these layers will undergo the most amount of stress. Figure 21 shows samples 2D and 3A. Refer to Table I for the layup configurations of these samples.

The compression testing conformed to the test specification mention above. The sandwich structures were subjected to the loading shown in Figure 22 during the 4-point testing. For the three point bending test, the load P was applied at the center of the specimen.

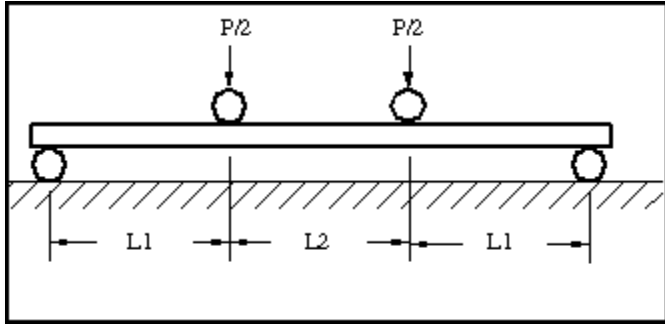


Figure 22: 4-Point Bending Test Set-Up

Figure 23 shows the carbon fiber behavior when the load is applied in the 3-point test. The fibers were close to breaking; however failure of this sample was due to the core material shearing during the test. The sample was able to withstand a load of about 400 lb. On average all of the samples subjected to a three point testing were able to withstand about the same load. The exception was the 2 X 2 samples which were made of a thicker core measuring 0.8 inches. On average, they failed at a lower load of 289.9 lb.

The following formula was used to carry out the stress calculations on both of the loading configurations.

$$F = \frac{P_{max} S(1-L/S)}{4(d-t)bt}$$



Figure 23: 3-Point Bending Test Result

Table 11: Variable Identifications

Symbol	Description	units
F	Facing ultimate stress	MPa [psi]
Pmax	Max force prior to failure	N [lb]
t	Layup thickness	mm [in]
b	Specimen width	mm [in]
C	Core thickness	mm [in]
d	Sandwich total thickness	mm [in]
L	Loading span length	mm [in]
S	Support span length	mm [in]
δ	Deflection	mm [in]

Table 12 shows the results for the three point bending test. Samples 2A as well as 3B have taken on the biggest loads at about 480 pounds of force. The configuration of sample 3B is the favorite thus far since it has taken the highest amount of stress at around 13,850 psi.

Table 12: Results from 3-Point Bending Test

Sample	P (lb)	d(in)	t(in)	c(in)	b(in)	S(in)	L	δ(in)	F (psi)
2A	479.126	0.570	0.035	0.5	3	5	0	0.065	10661.5
2B	415.039	0.570	0.035	constant				0.060	9235.4
3A	399.780	0.555	0.028					0.057	11483.0
3B	482.178	0.555	0.028					0.073	13849.7
2 X 2	289.917	0.845	0.023					0.167	6527.5

The second round of testing consisted of subjecting our test specimens to a four point bending test. This test requires that the load is spread between two points over a distance (L_2 in Figure 22). Our test specimen is 203.2 mm in length, allowing us to set a span of 152.4 mm between the supports. This configuration allowed us to set the loading points 50.8 mm apart, in other words, the loading points are set 25.4 mm from the center line of the test specimen (See Figure 22).

Table 13: Results from 4-Point Bending Test

Sample	P (lb)	d (in)	t (in)	c (in)	b (in)	S (in)	L (in)	δ(in)	F (psi)
2C	607.30	0.558	0.029	0.5	3	6	2	0.087	13195.57
2D	564.58	0.558	0.029	Constant				0.087	12267.24
2X2	619.51	0.875	0.038					0.159	6575.197

Table 13 shows the results from the four point bending test. Sample 2C was the sample able to take on the highest amount of stress at around 13ksi. This layup will provide the necessary strength required to accommodate a range of riders.

FLUID FLOW ANALYSIS

Aerodynamic analysis was done on the fairing using SolidWorks Flow Simulation. The primary output of the analysis is the CdA of the model, which is the product of the drag coefficient and frontal area. The input parameters for the analysis are summarized in Table 14. The surface roughness is an estimation based on reported values for fairing roughness by other HPV teams. The value used, 30 μ m, was made a little higher than estimates from other schools to account for the team's lack of experience in carbon fiber lay-up manufacturing.

Table 14: Fluid Analysis Parameters

Freestream pressure	14.7 psi
Freestream velocity	40mph
Fluid temperature	70°F
Surface Roughness	30 μ m

Every component of the final vehicle design was included in the solid model used for the flow analysis, with exception to the front and rear wheels. A simplified model of the rider was also included to ensure a more realistic result. Flow analyses was performed for each design iteration of the fairing. Based upon the flow analysis, the design was modified to reduce drag before running the analysis again. Figure 23 shows the last three iterations of the fairing design, and the corresponding reduction in CdA. The back portion of the fairing had a rise added to it in Iteration 2 to improve pressure recovery in that region. Iteration 3 added a bottom fairing, which brought about the greatest reduction in CdA. The CdA values for each design iteration are compared in Table 15. The aerodynamics department chose to use Iteration 2 for multiple reasons; the main reason was ease of manufacturing and repair. The flat surface of the belly pan is an ideal mounting surface, by adding a curved underside the steering assembly would be greatly affected. The result would be either mounting on a curved surface or mounting the bottom fairing over the steering system thus requiring the fairing to be removed every time a modification or repair needed to be made.

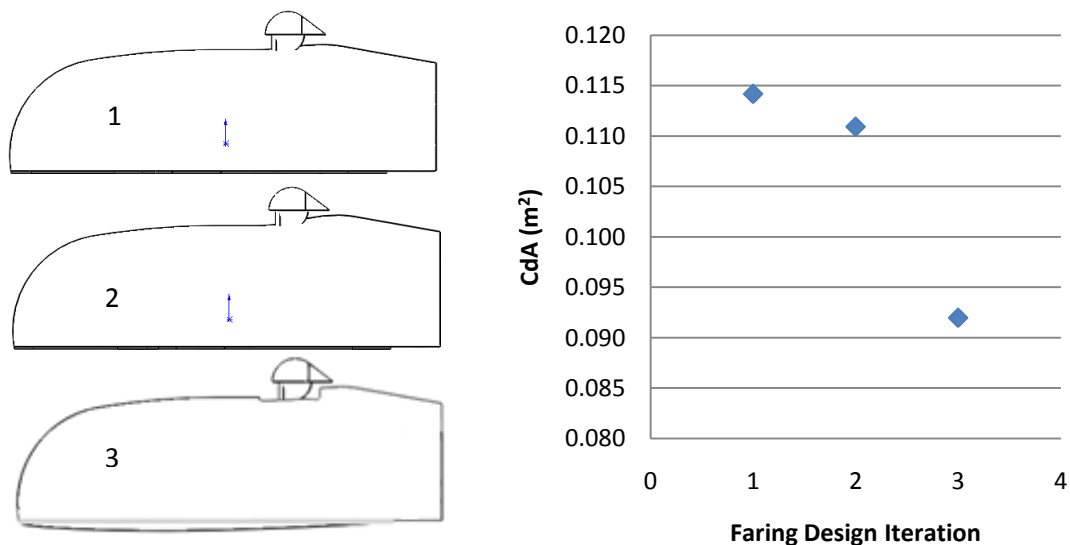


Figure 23: Change of CdA with each design iteration

Table 15: CdA comparison for each iteration compared with previous year's HPV

Design Iteration	Drag Force (N)	CdA (m ²)	CdA improvement from previous iteration
1	21.9	0.114	-
2	21.3	0.111	2.63%
3	17.6	0.092	17.12%

The pressure surface plot from the flow analysis is shown in Figure 24. The surface plot shows a favorable pressure gradient along the side of the fairing that goes past the widest point of the fairing. The pressure starts to increase at a plane just behind the rider's head. Because pressure and air velocity are inversely related by Bernoulli's law, we can therefore expect the air flow to accelerate from the nose until around the location of the rider's head. This behavior is desirable in order to delay the onset of turbulent flow which occurs when the boundary layer separates from the surface of the fairing. From the top view, there is a local deceleration of flow ahead of the rider's head. The rider will be wearing an aerodynamic helmet to reduce its contribution to drag.

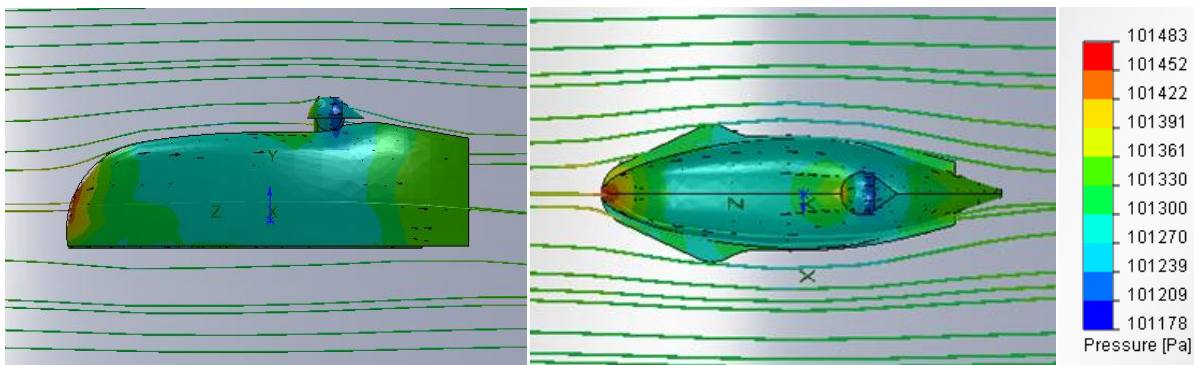


Figure 24: Pressure surface and flow trajectory plot from side and top views

CFD results are inherently highly optimistic, and are only used to provide a general idea of the change in drag with every design change. Turbulent flow is expected to occur significantly ahead of theoretical conclusions. Furthermore, ground effects have not been accounted for, which would most likely increase the drag of the vehicle. The CdA of the third iteration is compared with the previous year's HPV entry, which had a CdA of 0.24. The reduction comparison is tabulated in Table 16.

Table 16: CdA comparison with previous year's HPV

Design Iteration	CdA (m ²)	Reduction from previous year (CdA = 0.25)
3 - Final	0.092	61.67%

Cost Analysis

In addition to designing and manufacturing a human powered vehicle a proper cost analysis and business model is needed to obtain a business loan. Every aspect of designing and manufacturing needs to be accounted for in the cost analysis, including start-up capital investment for CNC machines, tools, and computers. The capital investment needed can be seen in Table 17. In addition to capital investment costs vehicle cost, and personnel cost tables were produced seen in Tables 18 and 19 respectively. Total monthly overhead was calculated assuming 40 hours/week and producing 5 vehicles per month seen in Table 20.

Table 17: Capital Investment

	Cost	Quantity	Total Cost
Design Team Computers	\$2,000.00	4	\$8,000.00
CNC Lathe	\$25,000.00	1	\$25,000.00
CNC Mill	\$25,000.00	1	\$25,000.00
Carbon Fiber Vacuum Pumps	\$400.00	3	\$1,200.00
Welding Machine	\$4,000.00	1	\$4,000.00
		Total	\$63,200.00

Table 18: Vehicle Costs

Materials	Unit Cost	Single Vehicle Cost		5 Vehicle Cost		10 Vehicle Cost	
		Quantity	Total Cost	Quantity	Total Cost	Quantity	Total Cost
Carbon Fiber	\$35.00	25	\$875.00	125	\$4,375.00	250	\$8,750.00
Epoxy (resin & hardener)	\$100.00	2	\$200.00	10	\$1,000.00	20	\$2,000.00
Vacuum Bagging Material	\$700.00	1	\$700.00	1	\$700.00	1	\$700.00
Vacuum Bag Sealant	\$200.00	1	\$200.00	1	\$200.00	1	\$200.00
Breather Fabric	\$200.00	1	\$200.00	1	\$200.00	1	\$200.00
Peel Ply Fabric	\$300.00	1	\$300.00	1	\$300.00	1	\$300.00
Aluminum	\$150.00	1	\$150.00	5	\$750.00	10	\$1,500.00
Aramid Honeycomb	\$600.00	1	\$600.00	5	\$3,000.00	10	\$6,000.00
G-10 Fiberglass sheet	\$200.00	1	\$200.00	5	\$1,000.00	10	\$2,000.00
Foam for Fairing Mold	\$500.00	1	\$500.00	1	\$500.00	1	\$500.00
Bicycle Components	\$2,000.00	1	\$2,000.00	5	\$10,000.00	10	\$20,000.00

Table 19: Labor and Design Team Costs

Labor	Hourly Rate	Quantity	Hours per week	Cost per Week
Carbon Fiber Lay Up Team (\$/hr)	\$18.00	4	40	\$2,880.00
Machinist	\$25.00	1	40	\$1,000.00
Welder	\$20.00	1	40	\$800.00
Supervisor	\$27.50	1	40	\$1,100.00
Assembly team	\$15.00	3	40	\$1,800
Design Team				
Supervisor	\$27.50	1	40	\$1,100.00
Design Engineers	\$25.00	4	40	\$4,000.00
Total Weekly Expenses				\$12,680.00

Table 20: Total Monthly Overhead for 5 Vehicles per Month

	Cost per Week	Quantity	Total Monthly Cost
Labor and Design Costs	\$12,680.00	4	\$50,720.00
Vehicle Cost	\$5,925.00	5	\$29,625.00
		Total	\$80,345.00

Costs for facilities, utilities, and physical plant were neglected due to varying costs throughout the country. The total monthly overhead is calculated for four weeks of work producing five complete vehicles. This produces a cost of \$16,069.00 per vehicle. This vehicle cost will be slightly marked up to produce a profit. Since most cars are at least \$15,000 add insurance, maintenance, and fuel costs per year and the price of the HPV is much more reasonable.

Citations

[1] Horowitz, Rickey M. *Trike Design 101, Part 1*. Version 7.0, www.hellbentcycles.com

[2] Wilson, G. David. Bicycling Science. Massachusetts: The MIT Press, 2004

2010 Human Powered Vehicle Challenge West

Sponsored by ASME and California State University, Northridge (CSUN)

Form 6: Vehicle Description

Due March 22, 2010

(Dimensions in inches, pounds)

Competition Location: California State University, Northridge

School name: California State University, Northridge

Vehicle name: N.E.D. 1.0

Vehicle number: 70

Vehicle type Unrestricted _____ Speed X _____

Vehicle configuration

Upright _____ Semi-recumbent X _____

Prone _____ Other (specify) _____

Frame material Carbon fiber composite belly pan with honeycomb core

Fairing material(s) Carbon fiber with Kevlar fabric sandwiched

Number of wheels 3

Vehicle Dimensions

Length 87.25 in. Width 45 in.

Height 46 in. Wheelbase 58 in.

Weight Distribution Front 60% Rear 40% Total 100%

Wheel Size Front 20" Rear 27.5"

Frontal area 674 in²

Steering Front X _____ Rear _____

Braking Front _____ Rear _____ Both X _____

Estimated Cd 0.21

Vehicle history (e.g., has it competed before? where? when?)

This vehicle is a clean sheet design and has not competed in any event.

